Green Chemistry

Enhancing Multifunctional Properties of Renewable Lignin Carbon Fiber via Defining Structure-Property Relationship Using Different Biomass Feedstock

Journal:	*Green Chemistry*
Manuscript ID	GC-ART-11-2020-003828.R2
Article Type:	Paper
Date Submitted by the Author:	16-Feb-2021
Complete List of Authors:	Li, Qiang; Texas A&M University System, Synthetic and Systems Biology Innovation Hub; Texas A&M University System, Plant Pathology and Microbiology Hu, Cheng; Texas A&M University System, Department of Plant Pathology and Microbiology Li, Mengjie; Texas A&M University System, Department of Plant Pathology and Microbiology Truong, Phuc ; Texas A&M University System, Soft Matter Facility Li, Jinghao; Texas A&M University System, Plant Pathology and Microbiology Lin, Hao-Sheng; Texas A&M University System, Department of Soil and Crop Science Naik, Mandar; Texas A&M University College Station, Department of Biochemistry and Biophysics Xiang, Sisi; Texas A&M University System Jackson, Brian; North Carolina State University, Horticultural Science; North Carolina State University Kuo, Winson; Texas A and M University System, Materials Characterization Facility Wu, Wenhao; Texas A and M University College Station, Department of Physics and Astronomy Pu, Yunqiao; Oak Ridge National Laboratory, Joint Institute of Biological Science, Biosciences Division Ragauskas, Arthur; The University of Tennessee Knoxville Yuan, Joshua; Texas A&M University System, Institute for Plant Genomics and Biotech

SCHOLARONE™
Manuscripts

Enhancing Multifunctional Properties of Renewable Lignin Carbon Fiber via Defining Structure-Property Relationship Using Different Biomass Feedstock

Qiang Li[1,2], Cheng Hu[1,2], Mengjie Li[1,2], Phuc Truong[3], Jinghao Li[1,2], Hao-Sheng Lin[1,4], Mandar T. Naik[5], Sisi Xiang[6], Brian E. Jackson[7], Winson Kuo[6], Wenhao Wu[8], Yunqiao Pu[9], Arthur J. Ragauskas[9,10,11], Joshua S. Yuan[1,2*]

[1]Synthetic and Systems Biology Innovation Hub, Department of Plant Pathology and Microbiology, Texas A&M University, College Station, TX 77843, USA

[2]Department of Chemical Engineering, Texas A&M University, College Station, TX 77843, USA

[3]Soft Matter Facility, Texas A&M University, College Station, TX 77843, USA

[4]Department of Soil and Crop Science, Texas A&M University, College Station, TX 77843, USA

[5]Department of Molecular Pharmacology, Physiology and Biotechnology, Brown University, Providence, RI 02903, USA

[6]Materials Characterization Facility, Texas A&M University, College Station, TX 77843, USA

[7]Department of Horticultural Science, North Carolina State University, Raleigh, NC 27695, USA

[8]Department of Physics and Astronomy, Texas A&M University, College Station, TX 77843, USA

[9]Joint Institute for Biological Sciences, Biosciences Division, Oak Ridge National Laboratory, Oak Ridge, TN 37831, USA

[10]Department of Chemical and Biomolecular Engineering, The University of Tennessee, Knoxville, TN 37996-2200, USA

[11]Department of Forestry, Wildlife and Fisheries, Center for Renewable Carbon, Institute of Agriculture, The University of Tennessee, Knoxville, TN 37996-2200, USA

*For correspondence: Joshua S. Yuan: syuan@tamu.edu

Abstract

Lignin has been explored extensively as a renewable precursor for carbon materials, considering its abundance as a major component of plant cell wall and its sustainability as a byproduct of both lignocellulosic biorefinery and paper-making industries. Despite the extensive efforts on defining process-property relationship, it remains largely unknown how lignin biosynthesis and its chemistry would impact on the resultant carbon fiber properties, for both mechanical and electroconductive performances. Such inadequate understanding fundamentally limited the feedstock design and selection to improve carbon fiber properties toward broader commercial application. Using lignin from a broad range of biomass feedstock for carbon fiber manufacturing, we have fundamentally explored the structure-function relationship between lignin chemistry and carbon fiber performance. Specifically, lignin extracted from hardwood (sugar maple), softwood (loblolly pine and red cedar), and herbaceous plant (corn stover and switchgrass) were used for carbon fiber manufacturing, considering the very different lignin structures from these feedstock. Linear regression models were established to define the relationship between carbon fiber mechanical properties with lignin structural characteristics. The results highlighted that the content of *β*-*O*-4 linkage correlates significantly with tensile strength and elastic modulus of lignin carbon fiber, indicating that the more linear *β*-*O*-4 linkage would promote carbon fiber mechanical performance. Moreover, electroconductive property is essential for broader energy device application of lignin-based carbon fiber, yet the mechanisms controlling its electroconductivity is largely unknown. We hereby demonstrated that a higher *β*-*O*-4 content also promotes electroconductivity of lignin carbon fiber. Microstructure analysis further revealed that the crystallite size and content of pre-graphitic turbostratic carbon structure in lignin-based carbon fiber was enhanced as the *β*-*O*-4 linkages increased. The content of *β*-*O*-4 linkage has shown a

strong correlation with crystallite content in linear regression model. This study thus revealed the underlying mechanisms regarding to how lignin structure *in planta* defines the resultant carbon fiber properties. Moreover, the study also highlighted the correlation between mechanical and electroconductive properties of lignin-based carbon fiber, both of which were defined by lignin structure.

Key words: lignin carbon fiber; structure-property relationship; *β*-*O*-4 linkage; biomass feedstock

1. Introduction

Lignin can be considered as the second most abundant biopolymer on earth and is a major byproduct in pulping and biorefining industries. Among the different renewable products derived from lignin, lignin-based carbon materials have significant and profound impact on energy and environment. On one side, as an abundant byproduct, the utilization of lignin as a precursor will reduce the carbon fiber cost, enable the broader applications of carbon fiber in automobile, wind turbine, and aerospace industries. Such broader application of light weight material will improve the energy efficiency and environmental sustainability for energy and other industrial sectors.[1-6] On the other side, the utilization of lignin for carbon fiber production will improve both sustainability and cost-effectiveness of the modern biorefining, considering the broad application, large volume, and high market value of carbon fiber.[7-9] Moreover, using renewable precursor like lignin for carbon fiber production represent a green and sustainable manufacturing for converting abundant industrial lignin waste into advanced materials. Despite the significant potential, the major challenge for the commercialization of lignin carbon fiber is the low performance as compared to the carbon fibers derived from traditional polyacrylonitrile (PAN) precursors.[8, 10] The underlying mechanisms for such low performance are still elusive, especially from plant lignin biosynthesis and biomass feedstock perspective.

Recent breakthroughs have focused on improving biomass processing to enhance lignin carbon fiber performance. For example, we have previously developed novel lignin fractionation methods using enzyme-mediator[7, 11, 12], dialysis tubes[7], and water[13, 14] to derive lignin with more uniform molecular weights, which had boosted lignin carbon fiber mechanical performance. Despite the progress, it is still not clear how inherent lignin structure as biosynthesized *in planta* will impact carbon fiber performance. Biomass characteristics and lignin chemical structure is largely defined

during plant cell wall thickening through several biosynthesis steps including monolignol biosynthesis, monolignol transportation outside of plasma membrane, and lignin polymerization (lignification).[15-21] The different ratio of monolignol and the following enzymatic and non-enzymatic coupling reactions would derive lignin with diverse chemical structures. Previous researches have focused on tailoring biomass processing to derive more processible carbohydrate,[22-28] yet very few researches focused on how the inherent chemical structure of lignin biosynthesized *in planta* could impact the resultant material performance. We aim to address this challenge by dissecting the relationship between carbon fiber properties and biomass characteristics using feedstock with diverse lignin structures.

In different biomass feedstock, including herbaceous plants, softwood and hardwood, lignin biosynthesis are known to produce different monolignol proportions and chemical linkage profiles.[29] For example, *ρ*-coumaryl alcohol is involved in lignin biosynthesis in herbaceous plants, forming *ρ*-hydroxyphenyl propane-type lignin (H lignin), whilst sinapyl alcohol is the major monolignol biosynthesized in angiosperm (hardwood) for the formation of syringyl-type lignin (S lignin) (Fig. 1). Different from the herbaceous plant and hardwood, gymnosperm (softwood) has guaiacyl-type lignin (G lignin) as the primary monolignol, which is biosynthesized from coniferyl alcohol (Fig. 1). Adding to the diverse monolignol structures, the three types of biomass feedstock also contain diverse linkage profiles, where hardwood typically contains more *β*-*O*-4 linkages than both herbaceous plants and softwood. Herbaceous plants, softwood and hardwood have all been widely used as feedstock for both biorefinery and pulp production.[30] In this study, we therefore focused on exploring how biomass characteristics regarding lignin structures define the microstructure and multi-functional properties of lignin carbon fiber. The new discovery will guide the feedstock development for both high value products and fuels.

Besides mechanical properties, another largely over-looked aspect for plant-derived renewable carbon fiber is the electroconductive property. Electroconductive property is an important consideration for the application of lignin-based carbon fiber in energy storage applications, including as carbonaceous electrodes for lithium-ion batteries and supercapacitors. [31] Despite the extensive studies of mechanical performance, it is still largely unknown what defines the electroconductive property of lignin-based carbon fiber and how the electroconductive performance is related to mechanical properties. Neither do we know if there is any strategy that could synergistically improve electroconductive and mechanical properties of lignin-based carbon fiber.

In this study, we therefore elucidated the relationship between lignin structure and multi-functional properties of carbon fiber using feedstock with very different biomass characteristics. Carbon fiber microstructure will be investigated to reveal the underlying mechanisms for improving electroconductive and mechanical properties. The mechanistic study has guided the development of strategies to synergistically improve electroconductive and mechanical properties, as well as delivering the lignin-based carbon fiber with comparable performance to PAN-based carbon fiber. The discovery will open up new avenues to design transformative feedstock for both biofuels and biomaterials and to enable sustainable and cost-effective biorefining and pulping industry.

2. Experimental

2.1 Materials

Different biomass of hardwood (sugar maple), softwood (red cedar and loblolly pine), and herbaceous plant (switchgrass and corn stover) were used in this research. All biomasses were

122 milled using a Wiley miller to pass a 60-mesh screen. The milled biomasses were then extracted
123 by benzene-ethanol extraction to remove extractives.[32] The extractive-free biomasses were stored
124 under 4 °C until utilization.
125 Polyacrylonitrile (PAN) with the molecular weight (MW) of 150,000 g/mol was obtained from
126 the Pfaltz & Bauer, USA. All other chemicals used in this research were purchased from Sigma–
127 Aldrich, USA.

128 **2.2 Lignin Preparation and Characterization**

129 ***Lignin Extraction***

130 Lignin was extracted by organosolv extraction using acetic acid as reported before.[33, 34] Briefly,
131 40 g of extractive-free biomass was treated with 90% aqueous acetic acid with the addition of 0.32%
132 sulfuric acid as catalyst. The liquid to solid ratio was 7:1 for all woody samples, while this ratio
133 was 10:1 for switchgrass and corn stover. The heating temperature was kept at around 118 °C in
134 an oil bath to keep acetic acid reflux. After 3-h treatment, the pretreatment mixture was cool down
135 and then filtrated to get a filtrate and biomass residue. The obtained filtrate was then concentrated
136 into about 100 mL by evaporation and followed by precipitation into deionized water and stirring
137 for 30 min. After centrifugation, three times washing with deionized water, centrifugation again
138 and lyophilization, fine powders of acetic acid lignin were obtained. The ash content of each lignin
139 sample was measured by pyrolyzing a certain amount of lignin in a muffle furnace (575 ± 25 °C)
140 for at least 4-h until no weight loss was measured. The very low ash content as shown in Table S2
141 indicated the high purity of all these lignin samples.

142 ***Fourier-transform infrared spectroscopy (FTIR)***

The possible carbonyl groups in the extracted lignin samples were analyzed using a Nicolet™ 380 FT-IR Spectrometer equipped with an OMNI-Sampler™ ATR sampling accessory. All lignin powders were grinded and dried to remove the moisture before the measurement. The spectra were recorded in the spectral range of 700–4000 cm^{-1} with a resolution of 4 cm^{-1}. For each measurement, 128 scans were collected for both background and sample. The peak at around 1720 cm^{-1} was assigned to the carbonyl group. The FTIR spectra are as shown in Fig. S2.

Gel permeation chromatography

The molecular weights of lignin were measured by using gel permeation chromatographic (GPC) analysis after acetylation as reported before.[7] In brief, lignin samples were acetylated using acetic anhydride and pyridine (1:1, v/v) at room temperature overnight under magnetic stirring. After the acetylation, ethanol was added and the mixture was evaporated using a rotatory evaporator. The acetylated lignin sample was then dissolved in tetrahydrofuran (THF). A membrane filter (0.45μm) was used to filter the solution before injecting for GPC analysis in an Agilent 1200 HPLC system (Agilent Technologies, Inc., Santa Clara, CA, US) equipped with three Waters Styragel columns (HR0.5, HR3, and HR5E; Waters Corporation, Milford, MA, USA) linked in series. An ultraviolet detector was employed for detection with wavelength setting at 270 nm. THF was used as the mobile phase and the flow rate was at 0.5 ml/min. The calibration curve was established by using a series of narrow range of polystyrene standards. The GPC results were presented in Table S3.

Two-dimensional Heteronuclear Single Quantum Coherence Nuclear Magnetic Resonance (2D HSQC NMR)

Lignin interunitary linkages were characterized under 2D HSQC NMR (Bruker AVANCE 500 MHz spectrometer equipped with a Cryoprobe). 150 mg of acetylated lignin was dissolved in 0.6 mL of DMSO-*d6* and placed in an NMR tube. Adiabatic 2D ^{1}H-^{13}C HSQC spectra were acquired and processed with Topspin 3.2 (Bruker Biospin) as described before.[11, 35] The obtained HSQC spectra were analyzed using the software MestReNova. The assignments and quantification of linkages were shown in Table S1. For the quantification of the relative difference in the lignin linkages, the well-resolved contours of Iβ, IIα, and IIIα (Fig. 7) were integrated using MestReNova software. The frequency of each linkage (Fig. 7B) was calculated using equation below:[35]

$$Frequency\ (\%) = \frac{I_x}{I_{\mathrm{I}\beta} + I_{\mathrm{II}\alpha} + I_{\mathrm{III}\alpha}} \times 100\ \%$$

Where I_x is the integration of the linkage to be calculated, and $I_{\mathrm{I}\beta}$, $I_{\mathrm{II}\alpha}$, $I_{\mathrm{III}\alpha}$ are the integrations of Iβ, IIα, and IIIα, respectively.

2.3 Carbon Fiber Fabrication

Precursor Fiber Spinning

Lignin was spun into fibers by a homemade wet spinning unit (Fig. 2). Lignin powders were firstly mixed with PAN at a weight ratio of 1:1, and then the mixture was dissolved in *N*,*N*-dimethylformamide (DMF) at 60 ^{o}C with the concentration of 10 %. Lignin/PAN dopes were sonicated using a Branson 1510 sonicator for 2-h before spinning to remove existed air bubbles. The dopes were then injected into a methanol coagulation bath (-20 ^{o}C) at a rate of 0.08 mL/min to form fibers. As-spun fibers were winded onto a rolling drum. After washing with deionized water, the fibers were cut and hanged under 15 g load until dry.

To evaluate the impact of different lignin-to-PAN ratios on the properties of the resultant fiber, lignin extracted from hardwood was mixed with PAN at two additional ratios of 65:35 and 75:25 with higher lignin content in the spinning dopes. Other conditions for wet spinning of the lignin/PAN dopes at 65:35 and 75:25 ratios were the same with that of lignin/PAN ratio at 1:1 (or 50:50).

Thermostabilization and Carbonization

As-spun lignin precursor fibers were thermostabilized and then carbonized into carbon fibers. The thermostabilization was carried out using a muffle furnace (GSL 1200X, MTI Corporation, Richmond, CA) at atmosphere. The heating was from room temperature to 250 ^{o}C at a heating rate of 1 ^{o}C/min. The holding time at 250 ^{o}C was 1 h. The thermostabilized fibers then underwent carbonization in a split tube furnace with vacuum system under nitrogen atmosphere (240 cm^3/min) (GSL 1600X, MTI Corporation, Richmond, CA). The temperature for carbonization was increased from room temperature to 1 000 ^{o}C with a heating rate of 5 ^{o}C/min and holding at 1000 ^{o}C for 1 h.

2.4 Carbon Fiber Characterization

Field Emission Scanning Electron Microscope (FE-SEM)

The morphologies of carbon fibers were observed under a Quanta 600F FE-SEM (FEI Company, Hillsboro, OR). Carbon fibers were coated with 10 nm iridium (Ir) prior the observation. The working distance was 10 mm, and the accelerating voltage applied was 5 kV. To get the morphologies of carbon fiber cross sections, fibers were mounted vertically on the SEM sample holder and then observed using the FE-SEM under the same conditions.

High-resolution transmission electron microscopy (HR-TEM)

TEM samples were prepared using a Tescan LYRA-3 Model GMH Ga^+ Focused Ion Beam Microscope with a standard FIB lift-out technique. The ion (Ga+) beam operated at 30 kV with a beam current ranging from 3nA down to 1nA was used to thin the membrane down to about 1μm. The sample was further polished to 1100 nm using successive currents of 1000, 300, and 100 pA following by final polish at 5 kV and 40pA. HR-TEM results were performed with an aberration-corrected scanning transmission electron microscope (S/TEM, Thermo Fisher Titan Themis Z 300) operated at 200 kV with a convergence semi-angle of 23.6 mrad. The microscope was aligned before every experiment by using a gold standard sample. The microscope was set to C2 aperture at 50um with beam current was set between 150~200 pA during the data acquisition.

Differential Scanning Calorimetry (DSC)

DSC was performed using a TA Q2500 system (TA Instruments, New Castle, DE) with two heating cycles under nitrogen atmosphere. Five milligram of thermostabilized fiber was placed in a pan and then heated from 0 ^oC to 400 ^oC. Both heating and cooling rates were 10 ^oC/min. The glass transition temperature (T_g) were derived from the second cycle of DSC analysis. All DSC thermograms were in Fig. S4.

Tensile Test

The mechanical performances of carbon fibers were measured under a TestResources universal mechanical tester (Shakopee, MN). A 2 N load cell with the resolution of 0.0001 N was used. Fibers were mounted on a sample holder made of paper board with the help of super glue. The sample holder was then fixed on two grippers. For the measurement, the displacement rate was set at 0.200 mm/min. The applied force (F) and the corresponding displacement (d) were monitored synchronously during the measurement. The original length (L) of fibers was measured by using a

vernier caliper. To get the area (A) of each fiber, the morphologies of the cross sections of carbon fibers were observed under aforementioned FE-SEM after the test. The area was then calculated using the software ImageJ®. Stress-strain curves can be plotted after getting stress (σ) and strain (ε) using the equations of $\sigma = F/A$ and $\varepsilon = d/L$, respectively. The tensile strength represented the maximum stress at fracture and the modulus of elasticity (MOE) was obtained from the slop of the elastic deformation region in a stress-strain curve. Elongation (%) was calculated by $d'/L \times 100$, where d' is the displacement at the fracture. For each sample, at least 15 fibers were measured to give an average result.

Electrical Conductivity Measurement

The electrical conductivity of the carbon fibers was measured using a Fluke 87 TRUE RMS multimeter. The measurement was as shown in Fig. 4B. A single fiber was fixed by silver paint (GC Electronics) onto a cover glass, and then the electrical resistance (R, Ω) of the fibers between two silver paints was measured with the multimeter at ambient atmosphere. The electrical conductivity (σ, S/m) was calculated from the equation of $\sigma = 1/\rho = L/(R \times A)$, where ρ is electrical resistivity (Ω.m), L (m) and A (m^2) are the length and the cross section area of the fiber as measured, respectively. The length (L) of the fiber was measured by using the aforementioned vernier caliper. To calculate the area (A) of fiber cross section, the diameter of each fiber was measured under a Zeiss Axiophot microscope after the conductivity test, and at least 25 points on one fiber were measured to give an average fiber diameter.

X-ray Diffraction (XRD)

XRD analysis of carbon fiber crystallite structures was performed under a Bruker D8 Discovery XRD (Bruker, Madison, WI). To avoid the orientation preference, carbon fibers were

ground into fine powders by an agate mortar and pestle before the measurement. X-ray resource was generated at 40 kV voltage and 40 mA current with Cu Ka wavelength (λ) of 1.542 Å. Scanning range (2θ) was from 8° to 55°, scanning step size was 0.05°, and scanning rate was set at 1.5°/min. The crystalline size (L_{hkl}) was calculated from Scherrer equation: $L = \frac{K\lambda}{\beta \cos\theta}$, where L is the crystalline size (nm); K is shape factor, set as 0.94 in this calculation; λ is the X-ray wavelength (1.542 Å); β is the full width at half maximum (FWHM) in radian; θ is the Bragg angle in degree. The distance between two crystalline lattices (d_{hkl}) was estimated using Bragg's law: $2d\sin\theta = \mathrm{n}\,\lambda$, where d is distance in nm; θ is the Bragg angle in degree; n is set as 1.

Raman Spectroscopy

The ground carbon fiber powder was mounted on a glass slide with the help of a double adhesive tape, and Raman spectra were taken under a Horiba Jobin-Yvon LabRam Raman Confocal Microscope with 633 nm laser, 10× magnification of objective lens, D0.3 filter, 200 μm confocal pinhole, 10 s exposure time, and 10 accumulations. D band (1348 cm^{-1}) and G band (1581 cm^{-1}) were deconvoluted by Guassian curve fitting method using Origin 9 software. The G/D ratios were calculated from the area ratios of these two bands.

3. Results and Discussion

3.1. Manufacturing carbon fiber from lignin derived from various biomass feedstock after mixing with PAN

In order to explore the impacts of lignin structure *in planta* on the carbon fiber performances, lignin from various types of feedstock with different biomass characteristics were extracted and then mixed with PAN for manufacturing carbon fibers. Corn stover, switchgrass, loblolly pine, red

cedar and sugar maple all have been extensively utilized as biomass feedstock in both biorefinery and pulping industries,[30] and they were selected in this research as representative feedstock of herbaceous plant, softwood and hardwood, respectively (Fig. 1). As an organosolv method, acetic acid extraction has been employed to fractionate lignin from these biomass samples. Acetic acid extraction has the advantages of the relatively mild reaction conditions at atmosphere pressure and lower temperature (around 118 ^{o}C, see experimental section), as well as the high purity of the lignin products as indicated by the low ash content (Table S2). Moreover, acetic acid lignin has been used to fabricate carbon fibers[36, 37] and activated carbon fibers[38] in established studies, proving the reliability of this lignin extraction for carbon fiber manufacturing.

To prepare lignin fibers, lignin extracted from these five feedstock was mixed with PAN at a 1:1 weight ratio and then dissolved in DMF to render a spinning dope with 10% concentration. Single fiber was formed under a customized wet-spinning set-up (Fig. 2A), where spinning dopes were injected into methanol coagulation bath (Fig. 2B) and then the formed single fibers were collected on a winding drum (Figs. 2C and 2D). As shown in Fig. 2D, as-spun precursor fibers had brownish color and were well aligned on the collection drum. The continuous length of the as-spun fibers can reach 300 meters, indicated the stability and reliability of the spinning technology. Moreover, we evaluated the fiber performance for lignin-to-PAN ratios from 1:1 (or 50%:50%) to 65%:35% and 75%:25% in order to evaluate if more PAN could be replaced by lignin. The increased lignin content led to deteriorated spinnability and decreased quality of the as-spun fiber (as shown in Fig. S6), indicating that lignin-to-PAN ratio at 1:1 was the optimal for replacing lignin with PAN toward carbon fiber manufacturing. The precursor fibers were subsequently subjected to thermostabilization at 250 ^{o}C and thereafter carbonization at 1000 ^{o}C to convert into carbon fibers. The morphologies of the carbon fibers were analyzed using a scanning electron

microscope (SEM). Several aspects of morphological features indicated the robustness and reliability of the manufacturing process.

First, morphological analysis of the prepared lignin-based carbon fibers showed high quality in terms of fiber geometrical structures. As shown in Figs. 3A1-E1, each lignin-derived carbon fiber was well separated with same orientated directions. Even though the surfaces of the carbon fibers had some indents along fibers (Figs. 3A2-E2), which could be rendered by polymer coagulation processed on the interfaces between the spinning dopes and the coarse interior faces of the injection needle, the cross sections of all carbon fibers were smooth and non-porous according the SEM analysis (Figs. 3A3-C3). These results suggested that the polymers of lignin and PAN were coagulated and interacted intimately with each other without significant void-defects formation in the coagulation process.[39, 40] In addition, all carbon fibers had similar average diameters around 36 μm (Figs. 3A4-E4), indicating the consistency of the resultant fibers and the stability and replicability of the customized wet spinning system. More importantly, unlike the previous lignin carbon fibers made by electrospinning,[11] each carbon fiber prepared through wet spinning was uniform in fiber axial direction and free of beads defects (Fig. 3), suggesting the robustness of this customized wet spinning technology. All these data of morphological analysis showed that the carbon fibers were with homogenous geometrical structures.

Second, the diameter distribution analysis suggested that the carbon fibers from different feedstock showed notable variations in spinnability, among which lignin from hardwood biomass showed the best spinnability. As shown in the histograms in Figs. 3A4-E4, carbon fiber made of lignin from sugar maple had narrower diameter distribution (ranging from 34 to 40 μm, Fig. 3E4) than that of red cedar (ranging from 32 to 40 μm, Fig. 3D4) and other biomass (loblolly pine, switchgrass and corn stover, ranging from 32 to 42 μm, Figs. 3A4-3C4, respectively). In addition,

the percentage for the most frequent 2 μm diameter range was 65.0 % for the carbon fiber made from the lignin of sugar maple (Fig. 3E4), which was much higher than that made from all other lignin of red cedar (50.0 %, Fig. 3D4), loblolly pine (35.0 %, Fig. 3C4), switchgrass (40.0 %, Fig. 3B4) and corn stover (37.5 %, Fig. 3A4). These results highlighted that lignin from sugar maple could improve the spinnability of the lignin, and thereby the uniformity in the diameters of carbon fibers. The improved spinnability could be attributed to lignin chemical structures and could correlate with the enhanced performances of carbon fibers, such as mechanical properties and electrical conductivity. We thereafter evaluated the carbon fiber performances and explored the relationship between lignin chemistry and lignin carbon fiber properties.

3.2. Mechanical properties of lignin-based carbon fibers from various biomass feedstock

Current lignin-based carbon fiber had significantly lower mechanical performances as compared to the traditional PAN-based carbon fibers, which could attribute to the chemistry of carbon fiber precursor. Tensile test revealed that the carbon fibers derived from sugar maple lignin had superior mechanical performances, which were even comparable with pure PAN-based carbon fibers. As shown in Fig. 4A-a, tensile test showed linear stress versus strain curves of lignin-based carbon fibers, and revealed elastic deformation behaviors of the carbon fibers before ultimate fracture.[41] From the stress-strain curves, modulus of elasticity (MOE, Fig. 4A-b) and tensile strength (Fig. 4A-c) were calculated from the slope of elastic deformation region and the stress at ultimate fracture, respectively. As shown in Fig. 4A-b, MOE of carbon fibers showed significant differences among hardwood, softwood, and herbaceous biomass. In particular, the carbon fibers made of lignin from sugar maple (hardwood) was 40.4 GPa, which was higher than that of carbon fibers made of lignin from both red cedar (37.7 GPa) and loblolly pine (36.2 GPa) (softwoods) and was much higher than switchgrass (33.8 GPa) and corn stover (28.5 GPa) (herbaceous plants).

Meanwhile, the tensile strength of carbon fiber made of sugar maple lignin (475 MPa) (hardwood) was about 1.2-fold higher than that made of red cedar lignin (404 MPa) and loblolly pine lignin (396 MPa) (softwood), and was 1.6- and 2.6-fold higher than that made of switchgrass lignin (299 MPa) and corn stover lignin (182 MPa) (herbaceous plants), respectively (Fig. 4A-c). In addition, the elongation of lignin-based carbon fibers increased from 1.07 % and 1.15 % for corn stover and switchgrass, respectively, to 1.35 % and 1.45 % for loblolly pine and red cedar, respectively, and further increased to 1.51% for sugar maple (Fig. 4A-d).

More importantly, the sugar maple lignin-derived carbon fiber even rendered comparable mechanical properties to that of the pure PAN-based carbon fibers. As shown in Figs. 4A-b to -d, the MOE of pure PAN-based carbon fiber was 40.5 GPa, which was similar with that of the sugar maple lignin-based carbon fiber (40.4 GPa). Both tensile strength (453 MPa) and elongation (1.40 %) of PAN-based carbon fiber were actually slightly lower than that of the sugar maple lignin-based carbon fiber. As compared to previous studies, for the lignin-based carbon fiber compared with the pure PAN-based carbon fiber prepared at the same thermostabilization and carbonization conditions, the sugar maple lignin-based carbon fiber in this study represented the lignin-based fibers with the best comparable performance to pure PAN-based carbon fiber (Fig. 4A-e and Table S5). All of these results suggested that carbon fiber made of lignin from hardwood had better mechanical properties than those from softwood and herbaceous plants. The tensile test indicated that lignin from different types of biomass could significantly impact carbon fiber mechanical performances.

3.3. Electroconductive properties of lignin-based carbon fibers from different biomass feedstock

The electrical conductivity of the resultant carbon fibers correlated to their mechanical performances. As shown in Fig. 5-a, a single carbon fiber was used as a resistance in an electrical loop to test its electrical conductivity. Carbon fiber was fixed on a cover glass by silver paint. When 3V voltage was applied, the bulbs connected to lignin carbon fibers derived from all biomass feedstock can be lighted (Figs. 5-b1 to -b5). Nevertheless, the brightness of the lighted bulb increased in the order of corn stover, switchgrass, loblolly pine, red cedar and sugar maple (Figs. 5-b1 to -b5). These results highlighted that carbon fiber made from sugar maple lignin had the best electrical conductivity as compared to those from other feedstocks. When the voltage was increased to 4.5V, the bulb connected to the carbon fiber made of sugar maple lignin became much brighter as compared with 3V voltage applied (Fig. 5-b6). In order to further understand the mechanisms underlying the differential electroconductivity, we further tested the electrical conductivity of the fibers before carbonization. The electrical conductivity of the thermostabilized fiber from sugar maple lignin was further visualized by lighting a bulb at 4.5V voltage. As shown in Fig. 5-b7, the bulb was completely off, indicating thermostabilized lignin polymers by themselves were electrical resistant. These data highlighted that the improved electrical conductivity of sugar maple lignin-based carbon fibers could be resulted from the enhanced carbon structures during the carbonization process.[42] In fact, the electrical conductivity of the carbon fiber made from sugar maple lignin was 14225 S/m as measured using a multimeter, which was higher than those of the carbon fibers made from both red cedar (13909 S/m) and loblolly pine lignin (13071 S/m), and was much higher than those made of both switchgrass (9405 S/m) and corn stover lignin (6585 S/m) (Fig. 5-c). The study again demonstrated that sugar maple (hardwood) lignin-based carbon fiber had the most improved electrical conductivity as compared to the lignin from softwoods and herbaceous plants. Moreover, the enhanced electroconductive property of

lignin carbon fiber was consistent with its enhanced mechanical properties. As shown in Fig. 5-d, linear regression model revealed that the well correlation between electrical conductivity and MOE ($R^2 = 0.916$, $p < 0.01$), tensile strength ($R^2 = 0.901$, $p < 0.01$), and elongation ($R^2 = 0.789$, $p < 0.05$), indicated that electroconductive performance of carbon fibers can be improved synergistically with the mechanical properties. The mechanistic study of these improvements was subsequently carried out by analyzing the crystallite carbon structure in lignin-based carbon fibers.

3.4. Microstructure of lignin carbon fiber determines the mechanical and electroconductive properties

The crystallite in lignin-based carbon fiber had been characterized as pre-graphitic turbostratic carbon structure,[7, 11] which was mainly comprised of more or less-bent crystallite layers with sp^2-hybridized carbon atoms.[43] The size and the content of the crystallite carbon in carbon fibers were analyzed using both X-ray diffraction (XRD) and Raman spectroscopy. First, XRD analysis revealed the improved crystallite size (L_{hkl}) in the carbon fibers made of sugar maple (hardwood) lignin as compared to other feedstock. As shown in Fig. 6A, the XRD diffractograms of all lignin carbon fibers had main peaks around the 2θ of 23.5°, displaying the reflection at (002) panel.[44] The thickness of the crystallite was calculated using Scherrer's equation. As shown in Fig. 6B, the crystallite size for the carbon fiber made of the sugar maple lignin was 1.256 nm, which was higher than that made from red cedar lignin (1.156 nm) and loblolly pine lignin (1.001 nm), and was much higher than that made from switchgrass lignin (0.971 nm) and corn stover lignin (0.894 nm). These data highlighted that carbon fiber made from hardwood lignin had larger crystallite size than those made from softwood and herbaceous plants. Second, Raman spectroscopy analysis further confirmed that the carbon fiber made from sugar maple (hardwood) lignin had increased pre-graphitic turbostratic carbon structures as compared to those from the softwood and herbaceous

feedstocks. As shown in Fig. 6C, besides the disordered D band carbon structure at around 1325 cm^{-1}, all lignin-based carbon fibers had clear G bands at around 1586 cm^{-1}, indicating the existence of the graphite-derived carbon structures.[7, 11] The integrated G/D ratio as shown in Fig. 6D was 0.565 for carbon fiber made from sugar maple lignin, whilst the G/D ratio was 0.526 and 0.498 for carbon fiber made from red cedar and loblolly pine lignin and 0.419 and 0.340 for carbon fiber made from switchgrass and corn stover, respectively. The increased G/D ratio in lignin carbon fiber suggested the increased content of the pre-graphitic turbostratic carbon structure.[11] However, the turbostratic carbon structure was observed under the HR-TEM for pure PAN carbon fiber but was not found for hardwood lignin/PAN based carbon fibers (Fig. S7), which could be attributed to very small size of the crystalline structures as characterized by XRD. Overall, the crystallite structure analysis by XRD and Raman spectroscopy revealed the enhanced turbostratic carbon structure in carbon fibers made of hardwood lignin as compared to softwood and herbaceous plants.

The results highlighted several mechanistic discoveries that could guide the future development of multi-functional lignin carbon fibers of high quality. First, microstructures define the quality of carbon fiber. The best-performing mechanical properties and electrical conductivity of the carbon fibers made from the sugar maple lignin could be attributed to the best turbostratic carbon structures as revealed by XRD and Raman spectroscopy. In other words, the enhanced microstructures could account for the superior mechanical and electroconductive properties of carbon fibers made from hardwood lignin. Second, the improvement of mechanical and electroconductive performance of carbon fibers can be improved synergistically based on enhanced microstructure. The results thus highlighted that improvement of microstructure could be as a universal approach to synergistically improve different properties of lignin-based carbon fiber. Third, the synergistic improvement of both mechanical properties and electrical conductivity

for hardwood lignin-derived carbon fiber indicated that hardwood lignin could serve as a superior precursor for multifunctional renewable carbon material. Overall, the carbon fibers made of hardwood (sugar maple) lignin had the best crystallite structure and performances as compared to those made of lignin from softwoods (red cedar and loblolly pine) and herbaceous plants (switchgrass and corn stover). The results opened a new avenue to further study what biomass characteristics could define the microstructure of lignin carbon fiber and therefore improve its multi-functional properties.

3.5. Explorative study revealed that *β-O*-4 linkage boosts lignin carbon fiber performances

The diverse mechanical and electroconductive properties for carbon fibers from various biomass feedstock with differential lignin characteristics allowed us to identify the key lignin chemical features defining carbon fiber performance. Such fundamental study will guide the future feedstock and process development to deliver high quality carbon fiber. In order to better understand how lignin chemistry and biomass characteristics define the lignin carbon fiber performance, comprehensive analyses of the interunitary linkages and monolignol composition derived from various biomass feedstock were carried out using 2D HSQC NMR.

Lignin in hardwood, softwood and herbaceous plant had different interunitary linkage profiles, partially resulted from different S, G and H units.[19] Using the 2D HSQC NMR technique, we have clearly observed the difference in the frequencies of uncondensed *β-O*-4 and condensed *β*-5 and *β-β* linkages among different types of biomass (Fig. 7). As displayed in Fig. 7A and Table S1, carbon-*α* in *β-O*-4, *β*-5 and *β-β* were assigned to the peaks of δC/δH 74.5/5.0 ppm, δC/δH 87.7/5.5 ppm and δC/δH 87.0/4.5 ppm, respectively.[11, 35] The frequencies of the linkages were expressed as per 100 aromatic rings of S, G, and H units, which were assigned to the peaks at δC/δH 103.8/6.70 ppm ($S_{2/6}$), δC/δH 111.3/6.80 ppm (G_2) and δC/δH 127.2/7.30 ppm ($H_{2/6}$), respectively

(Fig. S1 and Table S1).[35] As shown in Fig. 7B1, the main *β*-*O*-4 linkage (*β*-aryl ether) was higher in sugar maple (35.8 %) than those in both red cedar (31.6 %) and loblolly pine (30.1 %), and was much higher than that in switchgrass (26.9 %) and corn stover (22.7 %). Meanwhile, *β*-5 linkage (phenylcoumaran, in Fig. 7B2) were significantly higher in lignin from both red cedar (20.78 %) and loblolly pine (21.02 %) than those from sugar maple (5.00 %), switchgrass (4.58 %) and corn stover (5.41 %). The difference of *β*-5 among lignin from the latter three biomass was not significant. In addition, the content of *β*-*β* linkage was much lower than those of both *β*-*O*-4 and *β*-5 in all types of lignin. The *β*-*β* linkage content in red cedar (8.54 %) and loblolly pine (7.44 %) was much higher than those from the other three biomass. These results of the high *β*-*O*-4 and low *β*-5 in sugar maple lignin were not out of expectation. As compared to the predominant G unit content in softwood (e.g., loblolly pine and red cedar) lignin, hardwood lignin from the sugar maple had most S units with methoxyl on carbon-5 (C_5) position (Fig. S1). The higher S unit content could prefer R_β and $R_{O\text{-}4}$ radicals formation during radical coupling (Figs. S5A and S5B-a), attributing to the higher *β*-*O*-4 frequency in the sugar maple lignin. Interestingly, both herbaceous plants (e.g., switchgrass and corn stover) had significantly higher S unit content, yet lower *β*-*O*-4 frequency than that of softwoods (loblolly pine and red cedar) (Figs. 7B1 and S1A). Such variations could be due to the impact of processing technologies on ester linkage, instead of the content of a certain monolignol. The herbaceous plants have a significant amount of *p*CA and FA units (Fig. S1), which can form liable ester linkages in lignin.[45, 46] These liable ester linkages could be readily broken down under chemical processing like acetic acid extraction, rendering the decreased *β*-*O*-4 frequency in lignin extracted from the herbaceous plants. The similar results can be observed when comparing corn stover with switchgrass. Even though corn stover had higher S units than switchgrass (Fig. S1A), the lower *β*-*O*-4 frequency in corn stover could be due to the

higher content of *p*CA and FA units (Figs. 7B1 and S1A). Meanwhile, high *β*-5 in red cedar and loblolly pine lignin (softwood) could be resulted from its G units (Fig. S1) with vacant C_5 position, which could form more R5 radicals for *β*-5 radical coupling (Fig. S5B-b).

Overall, the frequencies of *β*-*O*-4 were found to be clearly different between various types of biomass, where hardwood lignin inherently had more *β*-*O*-4 than both softwood lignin and herbaceous plant lignin.

Traditionally, lignin content and composition were considered to be the key factors determining biomass saccharification efficiency.[22] However, the biomass feedstock characteristics determining the quality for carbon fiber are largely un-defined. Our recent study suggested that different feedstock lines and growth conditions within the same species could impact molecular weight, polydispersity, and functional groups, all of which can contribute to carbon fiber performance.[47] Additionally, our previous studies of fundamental structure-property relationship using fractionation technologies also revealed that lignin fraction with smaller PDI (higher uniformity), higher molecular weight, more *β*-*O*-4 linkage, and less hydroxyl groups could correlate with higher mechanical properties of the resultant carbon fiber.[7,11,13,14] Nevertheless, it remains unclear how a particular feedstock species could render the structure beneficial for carbon fiber manufacturing. Notably, the molecular weight and PDI of the lignin samples from the five species showed no significant differences among them, proving a perfect reductionist system to investigate the impact of biomass characteristics other than molecular weight and uniformity on carbon material properties (Fig. S3 and Table S3). We thereby carried out linear regression analysis of various carbon fiber properties in response to different biomass characteristics. Surprisingly, we have found that both mechanical properties (Fig. 8A) and electrical conductivity (Fig. 8B) correlated with the *β*-*O*-4 linkage profile. In particular, hardwood lignin with more *β*-*O*-4 linkages

had higher mechanical properties (Fig. 4) and electrical conductivity (Fig. 5c). First, mechanical properties, in particular the MOE and tensile strength fitted perfectly with *β-O*-4 linkage in a linear regression model. As shown in Figs. 8A1 and 8A2, the linear regressions of *β-O*-4 *vs.* MOE and tensile strength resulted in the correlation determination (R^2) at 0.982 and 0.936, respectively, both of which had *P* values less than 0.01. Meanwhile, the linear regressions of *β-O*-4 *vs.* elongation had R^2 at 0.749 and $P < 0.05$ (Fig. 8A3). In addition, the linear regression of *β-O*-4 *vs.* electrical conductivity resulted in R^2 of 0.783 with $P < 0.05$ (Fig. 8B). These linear regression analysis results suggested that it is lignin *β-O*-4 linkage determines the multi-functional properties of lignin-based carbon fiber. Therefore, increasing *β-O*-4 content boosted the performance of lignin-based carbon fibers, the MOE and tensile strength in particular.

Considering the increased crystallite carbon structures in carbon fiber as measured by XRD and Raman spectroscopy (Fig. 6), we further analyzed the correlation relationship between *β-O*-4 linkage and carbon fiber crystallite structures. As shown in Fig. 8C, *β-O*-4 linkage had significant positive linear correlation with both the crystallite size (L_{hkl}, R^2 0.704 and $P < 0.05$) and the crystallite content (G/D ratio, R^2 0.878 and $P < 0.01$), indicating that *β-O*-4 linkage in lignin polymer could enhance the crystallite formation, in particular forming more crystallite carbon structures. All of these results thus revealed that lignin polymer with more *β-O*-4 linkage could enhance the crystallite formation and thereby boost the mechanical and electroconductive performances of the resultant carbon fibers.

The molecular mechanism for *β-O*-4 linkage to enhance the carbon fiber performance could lie in the flexibility of lignin polymer chain.[48-50] Lignin with more *β-O*-4 linkage bonded by C-O-C uncondensed links could be more flexible. Lignin polymer with improved flexibility would result in better aligned polymer orientations under stretching force loaded on precursor fibers by

winding system during the coagulation process in wet spinning (see Fig. 2). Moreover, DSC analysis revealed that hardwood (sugar maple) lignin-based fibers had lower glass transition temperature (T_g) than both softwood (red cedar and loblolly pine) and herbaceous plant (switchgrass and corn stover) lignin-based fibers (Fig. S4), indicating the improved miscibility of lignin molecules with guest PAN molecules.[11, 14] The improved miscibility also suggested that *β*-*O*-4 linkage increased the flexibility of lignin polymers, as the aligned polymers with similar orientation could enhance the interactions between each other or with other guest polymers like PAN.[49] This improvement of lignin polymer orientations and polymer-polymer interactions in precursor fibers could enhance the formation of the pre-graphite turbostatic carbon structures in carbon fiber,[8, 11, 39] which would account for the boosted mechanical performance and electrical conductivity of carbon fibers.

In summary, using feedstock with diverse biomass characteristics, we have defined the relationship between lignin chemistry and carbon fiber performance. Lignin polymer formed through different biosynthesis pathways in various biomass feedstock with inherently different chemical features could be favorable for making quality carbon fiber with enhanced mechanical and electroconductive performances. Lignin structures with high *β*-*O*-4 content could be manipulative through the regulation of the biosynthesis pathways, in particular the biosynthesis of monolignols.[51, 52] This research thereby demonstrated that such manipulation of lignin engineering in biomass to regulate lignin structures toward favorable *β*-*O*-4 linkages for carbon fiber production could not only facilitate biomass processing, but also has the potential to transform bioeconomy of lignocellulosic biorefinery and pulping mills by upgrading lignin byproducts into high value products like carbon fibers.

4. Conclusion

Lignin carbon fiber is still struggling for commercialization due to the challenge in poor performance. In this study, we presented a new concept addressed on the challenge that the quality of lignin carbon fiber is possible to be boosted through the regulation of lignin chemical structures in biomass feedstock. The concept was built on the finding that hardwood (sugar maple) lignin with more *β*-*O*-4 linkage than both softwood (red cedar and loblolly pine) and herbaceous plants (switchgrass and corn stover) resulted in carbon fiber with enhanced mechanical properties and electrical conductivity. Fundamental understanding of why hardwood lignin leads to the best mechanical and electroconductive performances of carbon fiber was demonstrated by XRD and Raman spectroscopy, which the pre-graphite turbostractic carbon structures in carbon fibers made from hardwood lignin were significantly improved. Furthermore, the relationship between lignin linkages and carbon fiber performances were evaluated by scatter plots. The *β*-*O*-4 linkage in lignin showed significantly linear correlation with the crystallite structure and the performances of lignin-based carbon fibers, particularly the MOE and tensile strength. Such correlation could guide the design of chemical processing of lignin molecular structures toward high quality lignin-based carbon. More importantly, the new concept presented in this research shed light on lignin carbon fiber production that the regulation of lignin chemical structures through the manipulation of lignin monolignol biosynthesis pathway *in planta* for high *β*-*O*-4 linkage could significantly boost carbon fiber performances. With the implementation of high *β*-*O*-4 linkage in lignin, the bioeconomy of both lignocellulosic biorefinery and pulping industry could be thus transformed by concurrently maximize cellulose fiber production and lignin-derived high value carbon materials.

Acknowledgements

The authors would like to thank Dr. Anup K. Bandyopadhyay in Department of Materials Science and Engineering (MSEN), Texas A&M University for his assistant of DSC and XRD characterizations and Dr. Thomas C. Stephens in Microscopy Image Center (MIC), Texas A&M University for his assistance for SEM. The authors also acknowledge the funding supports of Texas A&M Energy Institute Seed Grant to J.S.Y. and DOE EERE BETO grants (DE-EE0007104, DE-EE0006112, and DE-EE0008250) to J.S.Y.

Conflict of Interest

The authors declare no competing financial interests.

Author contributions

Q.L. and J.S.Y. designed the experiments. Q.L., C.H., M.L. and H.-S.L. carried out lignin extraction and fiber fabrication. Q.L. did lignin and the resultant carbon fiber characterizations with the assistances from P.T. on DSC, W.W. on electrical conductivity measurement, and M.T.N. on HSQC. B.E.J. provided all wood samples for this research. Y.P. did GPC characterization. Y.P. and A.J.R. supervised Q.L. on all NMR analyses presented in this paper. J.L. helped Q.L. with FTIR characterization of all lignin samples. W.K. and S.X. did HR-TEM characterizations of all carbon fibers. Q.L. and J.S.Y. discussed the results. Q.L. wrote the manuscript and J.S.Y. revised it. All authors contributed to the scientific discussions and comments on the manuscript.

Reference

1. Lynd, L.R. et al. How biotech can transform biofuels. *Nat. Biotechnol.* **26**, 169 (2008).

2. Mosier, N. et al. Features of promising technologies for pretreatment of lignocellulosic biomass. *Biores. Technol.* **96**, 673-686 (2005).

3. Wyman, C.E. Biomass ethanol: Technical progress, opportunities, and commercial challenges. *Ann. Rev. Energy Environ.* **24**, 189-226 (1999).

4. Lynd, L.R., Cushman, J.H., Nichols, R.J. & Wyman, C.E. Fuel ethanol from cellulosic biomass. *Science* **251**, 1318-1323 (1991).

5. Menon, V. & Rao, M. Trends in bioconversion of lignocellulose: Biofuels, platform chemicals & biorefinery concept. *Prog. Energy Combus. Sci.* **38**, 522-550 (2012).

6. Cherubini, F. The biorefinery concept: Using biomass instead of oil for producing energy and chemicals. *Energy Conver. Manag.* **51**, 1412-1421 (2010).

7. Li, Q. et al. Molecular weight and uniformity define the mechanical performance of lignin-based carbon fiber. *J. Mater. Chem. A* **5**, 12740-12746 (2017).

8. Baker, D.A. & Rials, T.G. Recent advances in low-cost carbon fiber manufacture from lignin. *J. Appl. Polym. Sci.* **130**, 713-728 (2013).

9. Li, Q., Ragauskas, J.A., Yuan, J.S. Lignin carbon fiber: The path for quality. *Tappi J.* ***16***, 107-108 (2017).

10. Mainka, H. et al. Lignin – an alternative precursor for sustainable and cost-effective automotive carbon fiber. *J. Mater. Res. Technol.* **4**, 283-296 (2015).

11. Li, Q. et al. Quality carbon fibers from fractionated lignin. *Green Chem.* **19**, 1628-1634 (2017).

12. Li, Q. et al. Microstructure defines the electroconductive and mechanical performance of plant-derived renewable carbon fiber. *Chemical Commun.* **55**, 12655-12658 (2019).

609 13. Li, Q. et al. Tuning hydroxyl groups for quality carbon fiber of lignin. *Carbon* **139**, 500-511
610 (2018).
611 14. Li, Q. et al. Non-solvent fractionation of lignin enhances carbon fiber performance.
612 *ChemSusChem* **12**, 3249-3256 (2019).
613 15. Boerjan, W., Ralph, J. & Baucher, M. Lignin biosynthesis. *Ann. Rev. Plant Biol.* **54**, 519-546
614 (2003).
615 16. Terashima, N. & Fukushima, K. Heterogeneity in formation of lignin—XI: An
616 autoradiographic study of the heterogeneous formation and structure of pine lignin. *Wood Sci.*
617 *Technol.* **22**, 259-270 (1988).
618 17. Higuchi, T. Lignin biochemistry: Biosynthesis and biodegradation. *Wood Sci. Technol.* **24**, 23-
619 63 (1990).
620 18. Weng, J.-K., Li, X., Bonawitz, N.D. & Chapple, C. Emerging strategies of lignin engineering
621 and degradation for cellulosic biofuel production. *Curr. Opin. Biotechnol.* **19**, 166-172 (2008).
622 19. Ralph, J. et al. Lignins: Natural polymers from oxidative coupling of 4-hydroxyphenyl-
623 propanoids. *Phytochem. Rev.* **3**, 29-60 (2004).
624 20. Jing-Ke, W. & Clint, C. The origin and evolution of lignin biosynthesis. *New Phytol.* **187**, 273-
625 285 (2010).
626 21. Sibout, R. & Höfte, H. Plant Cell Biology: The ABC of monolignol transport. *Curr. Biol.* **22**,
627 533-535 (2012).
628 22. Chen, F. & Dixon, R.A. Lignin modification improves fermentable sugar yields for biofuel
629 production. *Nat. Biotechnol.* **25**, 759 (2007).
630 23. Yoo, C.G. et al. Significance of lignin S/G ratio in biomass recalcitrance of *populus*
631 *trichocarpa* variants for bioethanol production. *ACS Sustain. Chem. Eng.* **6**, 2162-2168 (2018).

24. Thomas, V.A. et al. Comparative evaluation of populus variants total sugar release and structural features following pretreatment and digestion by two distinct biological systems. *Biotechnol. Biofuels* **10**, 292 (2017).

25. Mansfield, S.D., Kang, K.-Y. & Chapple, C. Designed for deconstruction – poplar trees altered in cell wall lignification improve the efficacy of bioethanol production. *New Phytol.* **194**, 91-101 (2012).

26. Van Acker, R. et al. Improved saccharification and ethanol yield from field-grown transgenic poplar deficient in cinnamoyl-CoA reductase. *Proc. Nat. Aca. Sci.* **111**, 845-850 (2014).

27. Huntley, S.K., Ellis, D., Gilbert, M., Chapple, C. & Mansfield, S.D. Significant increases in pulping efficiency in C4H-F5H-transformed poplars: Improved chemical savings and reduced environmental toxins. *J. Agric. Food Chem.* **51**, 6178-6183 (2003).

28. Wagner, A. et al. Syringyl lignin production in conifers: Proof of concept in a Pine tracheary element system. *Proc. Nat. Aca. Sci.* **112**, 6218-6223 (2015).

29. Vanholme, R., Demedts, B., Morreel, K., Ralph, J. & Boerjan, W. Lignin biosynthesis and structure. *Plant Physiol.* **153**, 895-905 (2010).

30. 2016 Billion-Ton Report. http://energy.gov/eere/bioenergy/2016-billion-ton-report.

31. Chatterjee, S., Clingenpeel, A., McKenna, A., Rios, O. & Johs, A. Synthesis and characterization of lignin-based carbon materials with tunable microstructure. *RSC Adv.* **4**, 4743-4753 (2014).

32. Ma, X.J. et al. Lignin removal and benzene–alcohol extraction effects on lignin measurements of the hydrothermal pretreated bamboo substrate. *Biores. Technol.* **151**, 244-248 (2014).

33. Pan, X.-J., Sano, Y., Nakashima, H. & Uraki, Y. Atmospheric acetic acid pulping of rice straw (1) Pulping conditions and properties of pulp. *Japan Tappi J.* **52**, 408-415 (1998).

655 34. Pan, X. & Sano, Y. Fractionation of wheat straw by atmospheric acetic acid process. *Biores.*
656 *Technol.* **96**, 1256-1263 (2005).
657 35. Mansfield, S.D., Kim, H., Lu, F. & Ralph, J. Whole plant cell wall characterization using
658 solution-state 2D NMR. *Nat. Protocols* **7**, 1579-1589 (2012).
659 36. Kubo, S., Uraki, Y. & Sano, Y. Preparation of carbon fibers from softwood lignin by
660 atmospheric acetic acid pulping. *Carbon* **36**, 1119-1124 (1998).
661 37. Uraki, Y., Kubo, S., Nigo, N., Sano, Y. & Sasaya, T. Preparation of Carbon Fibers from
662 Organosolv Lignin Obtained by Aqueous Acetic Acid Pulping. *Holzforschung* **49**, 343-350 (1995).
663 38. Uraki, Y., Nakatani, A., Kubo, S. & Sano, Y. Preparation of activated carbon fibers with large
664 specific surface area from softwood acetic acid lignin. *J. Wood Sci.* **47**, 465-469 (2001).
665 39. Erik, F., M., S.L., Denis, I., M., S.J. & R., B.M. Carbon Fibers: Precursor systems, processing,
666 structure, and properties. *Angew. Chem. Int. Ed.* **53**, 5262-5298 (2014).
667 40. Bell, J.P. & Dumbleton, J.H. Changes in the structure of wet-spun acrylic fibers during
668 processing. *Textile Res. J.* **41**, 196-203 (1971).
669 41. Arola, S., Malho, J.-M., Laaksonen, P., Lille, M. & Linder, M.B. The role of hemicellulose in
670 nanofibrillated cellulose networks. *Soft Matt.* **9**, 1319-1326 (2013).
671 42. Behabtu, N. et al. Strong, light, multifunctional fibers of carbon nanotubes with ultrahigh
672 conductivity. *Science* **339**, 182-186 (2013).
673 43. Frank, E., Hermanutz, F. & Buchmeiser, M.R. Carbon fibers: precursors, manufacturing, and
674 properties. *Macromol. Mater. Eng.* **297**, 493-501 (2012).
675 44. Nar, M. et al. Superior plant based carbon fibers from electrospun poly-(caffeyl alcohol) lignin.
676 *Carbon* **103**, 372-383 (2016).

677 45. Grabber, J.H., Hatfield, R.D., Lu, F. & Ralph, J. Coniferyl ferulate incorporation into lignin
678 enhances the alkaline delignification and enzymatic degradation of cell walls. *Biomacromolecules*
679 **9**, 2510-2516 (2008).
680 46. Wilkerson, C.G. et al. Monolignol ferulate transferase introduces chemically labile linkages
681 into the lignin backbone. *Science* **344**, 90-93 (2014).
682 47. Li, Q. et al. Discovering biomass structural determinants defining the properties of plant-
683 derived renewable carbon fiber. *iScience* **23**, 101405 (2020).
684 48. Bosch, A.T., Maissa, P. & Sixou, P. Effect of the flexibility on the phase transition of polymeric
685 liquid crystals. *Phy. Lett. A* **94**, 298-300 (1983).
686 49. Kubo, S. & Kadla, J.F. Poly(ethylene oxide)/organosolv lignin blends: Relationship between
687 thermal properties, chemical structure, and blend behavior. *Macromolecules* **37**, 6904-6911 (2004).
688 50. Uraki, Y. et al. Thermal mobility of *β*-*O*-4-type artificial lignin. *Biomacromolecules* **13**, 867-
689 872 (2012).
690 51. Aymerick, E. et al. Biosynthesis and incorporation of side-chain-truncated lignin monomers to
691 reduce lignin polymerization and enhance saccharification. *Plant Biotechnol. J.* **10**, 609-620
692 (2012).
693 52. Ruben, V. et al. Metabolic engineering of novel lignin in biomass crops. *New Phytol.* **196**, 978-
694 1000 (2012).
695

696

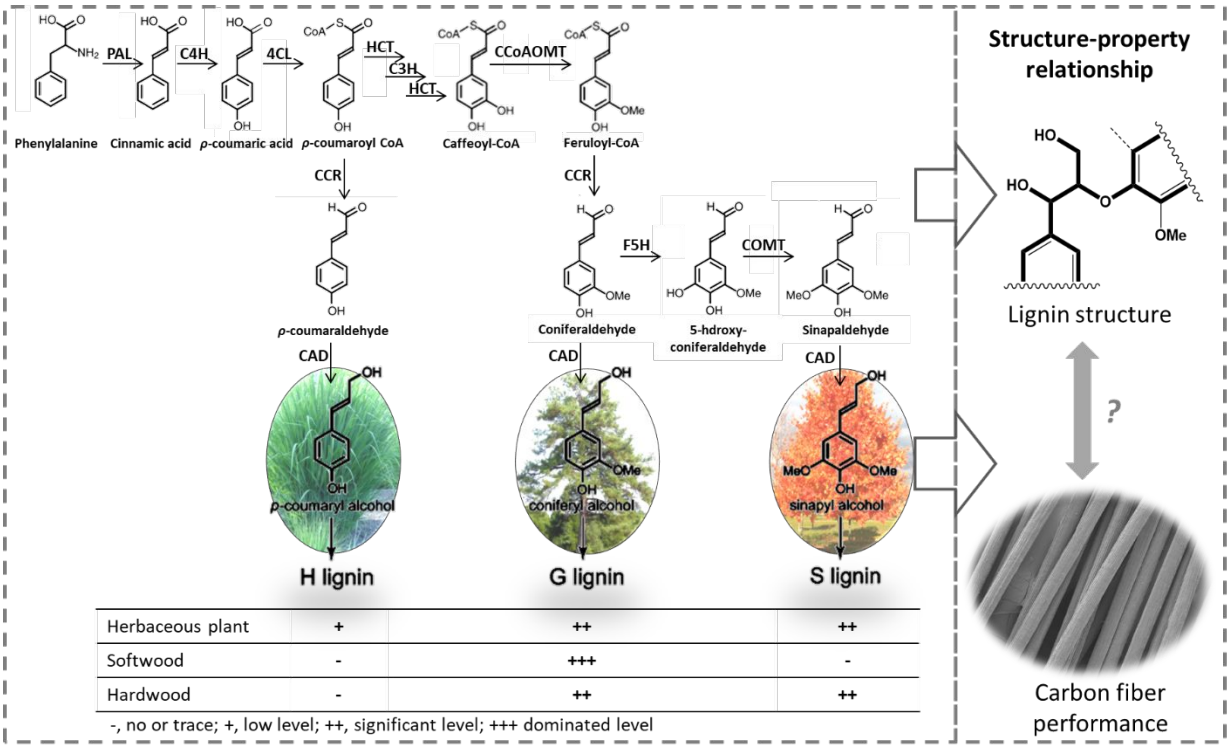

697

698 Fig. 1. The general schema of the study to use lignin from different feedstock to reveal the
699 structure-property relationship between lignin chemical structure and carbon fiber performance.
700 H, *p*-hydroxyphenyl propane; G, guaiacyl; S, syringyl.

701

702

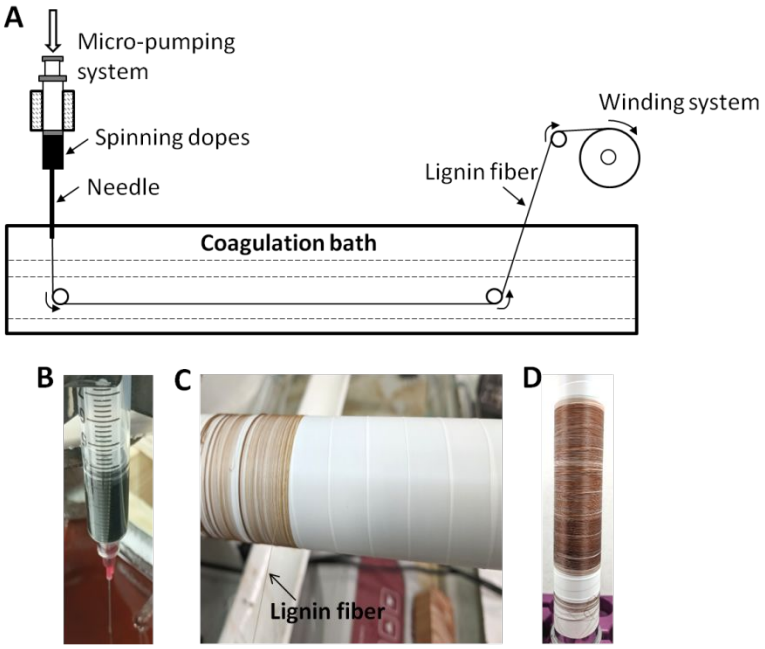

703

704 Fig. 2. Lignin fiber spinning set-up. A, spinning dopes were extruded by a micro pump through a
705 needle immersed in a coagulation bath, and the formed fiber was continuously collected on the
706 winding drum. B, close-up view of fiber formation, where lignin fiber was pulled out when lignin
707 solution was pumped into methanol/DMF coagulation bath. C, a single fiber out of coagulation
708 bath was collected on the winding drum. D, the collected as-spun lignin fibers.

709

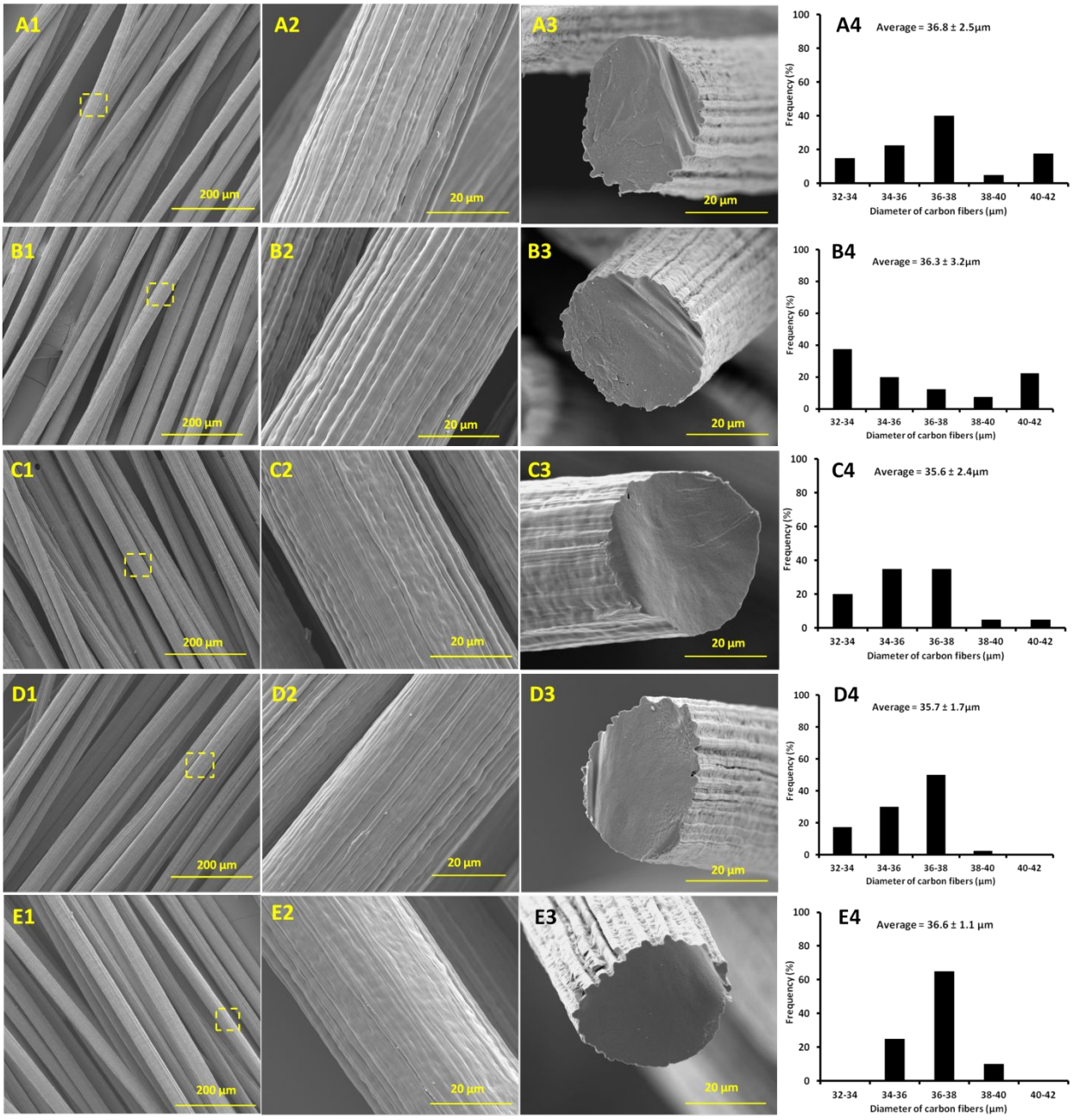

Fig. 3. SEM images of the surfaces and cross sections of carbon fibers. Panel A, B, C, D and E are corn stover, switchgrass, loblolly pine, red cedar and sugar maple, respectively. The histograms in the Panel 4 are the diameters and diameter distributions of carbon fibers.

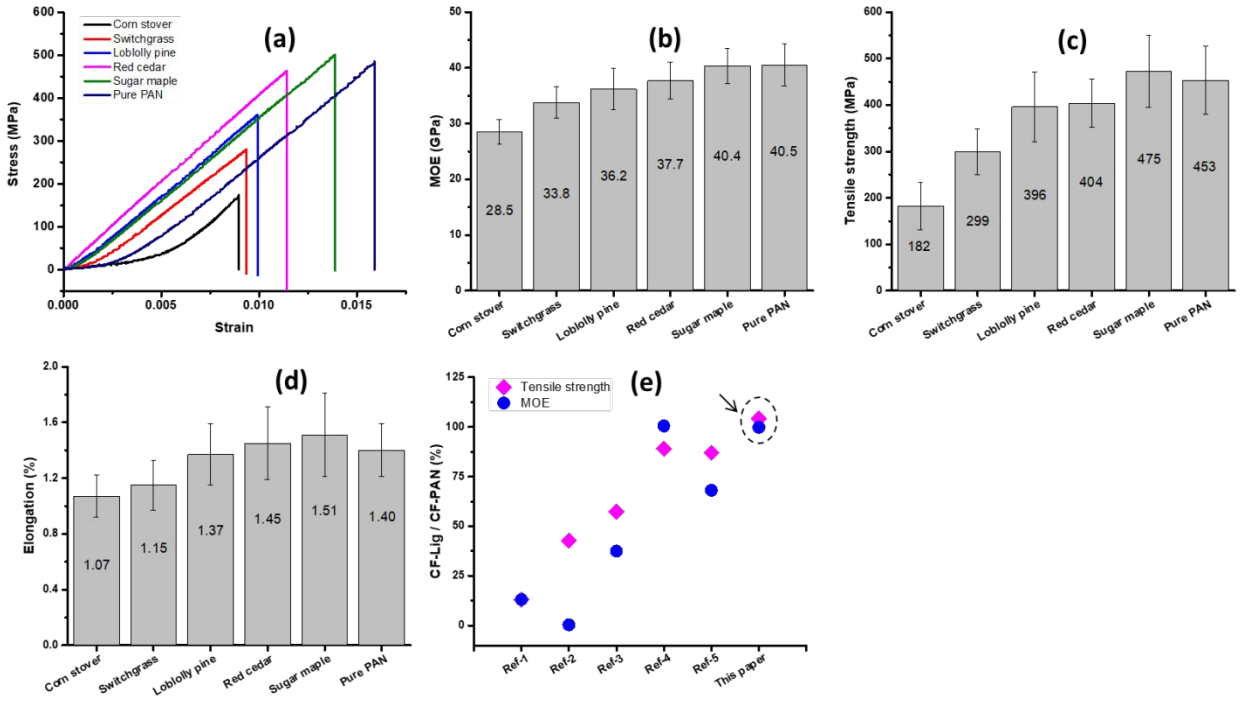

Fig. 4, Mechanical properties of lignin-based carbon fibers. a, representative stress-strain curves of carbon fibers; b, modulus of elasticity (MOE); c, tensile strength; d, elongation; e, the comparison of lignin-based carbon fiber (CF-Lig) with pure PAN carbon fiber (CF-PAN) as obtained in this study and reported in other literatures. In the Panel A-e, the Y-axis CF-Lig/CF-PAN represented the percentage of CF-Lig mechanical properties to that of the CF-PAN, and the references-1 to -5 were Lin et al (2012), Thunga et al (2014), Ding et al (2016), Liu et al (2017), and Jin et al (2018), respectively. The arrow and dashed circle highlighted our data. The calculations of the data in Panel e were given in Table S5.

729

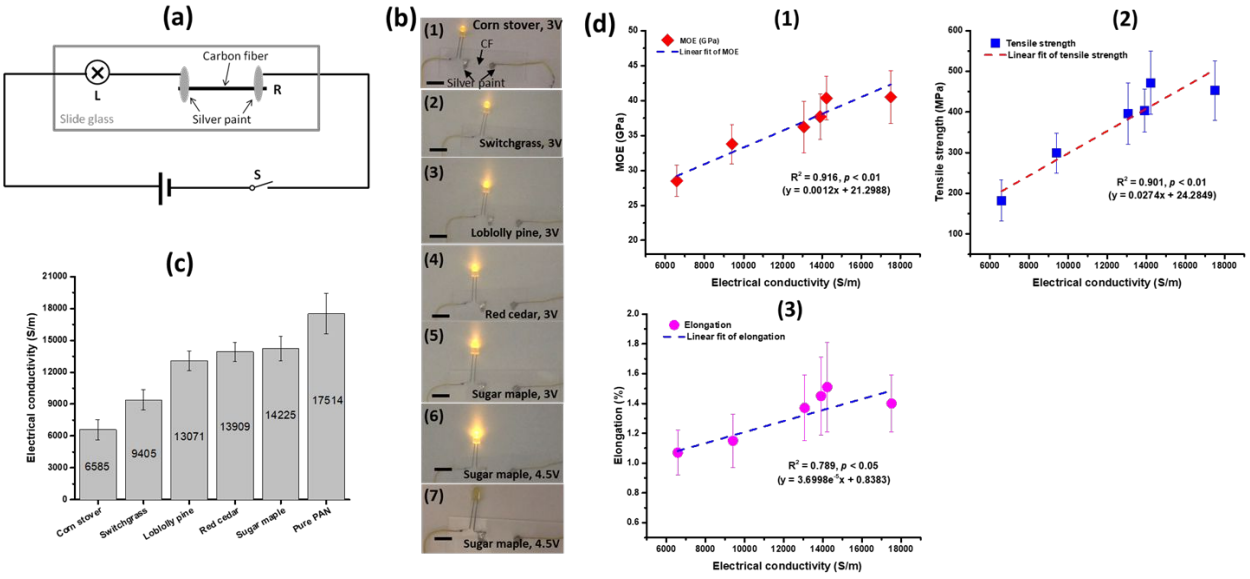

730

731 Fig. 5. Electrical conductivity of lignin-based carbon fibers. a, lignin carbon fiber as a resistance
732 in the circuit; b, the bulbs lighted at different voltage with carbon fibers as resistances; b-1 to b-5
733 were lighted at 3V, which were derived from corn stover, switchgrass, loblolly pine, red cedar and
734 sugar maple, respectively; b-6 was sugar maple lignin carbon fiber lighted at 4.5V. The
735 thermostabilized fiber of lignin from sugar maple was used as control (b-7); c, the electrical
736 conductivity of lignin-based carbon fibers as measured by a multimeter; d, linear correlation
737 relationships between electrical conductivity and mechanical performances. d1 to d3 are
738 correlations of electrical conductivity with MOE, tensile strength, and elongation, respectively.

739

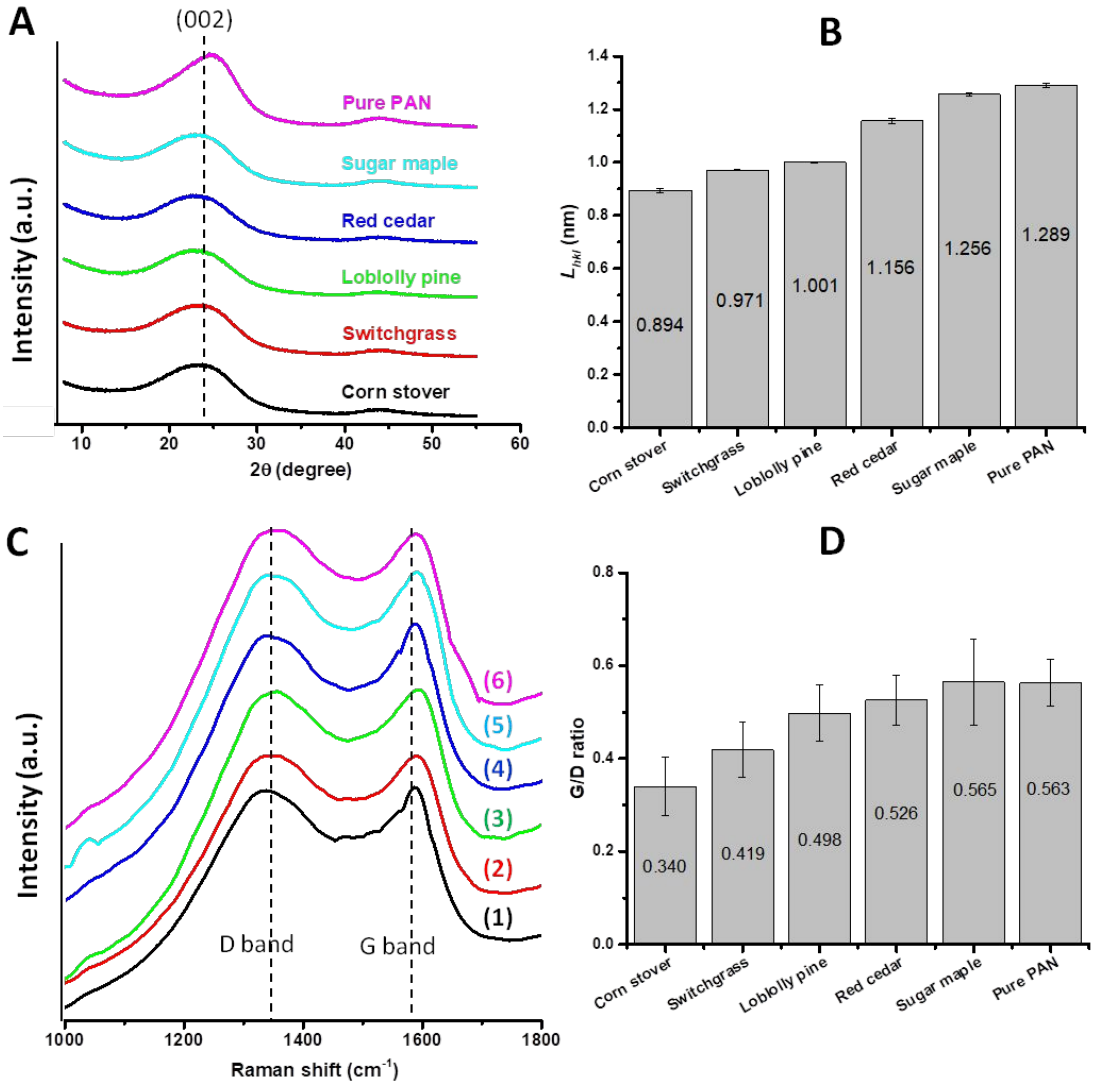

740

741 Fig. 6. Characterization of the crystallite structures in carbon fibers by XRD (A and B) and Raman
742 microscopy(C and D). A, XRD diffractograms of carbon fibers made of lignin derived from
743 different biomass feedstock and pure PAN; B, the crystallite size (L_{hkl}) in carbon fibers as
744 calculated from the Scherrer equation; C, Raman microscopy spectra of carbon fibers, where C1-
745 C6 were corn stover, switchgrass, loblolly pine, red cedar, sugar maple and pure PAN,
746 respectiverly. The left peak in panel C around 1330 cm^{-1} represented D band, and the right peak
747 around 1595 cm^{-1} was G band; D, the G/D ratios of carbon fibers as calculated from the G and D
748 bands from Raman microscopy.

749

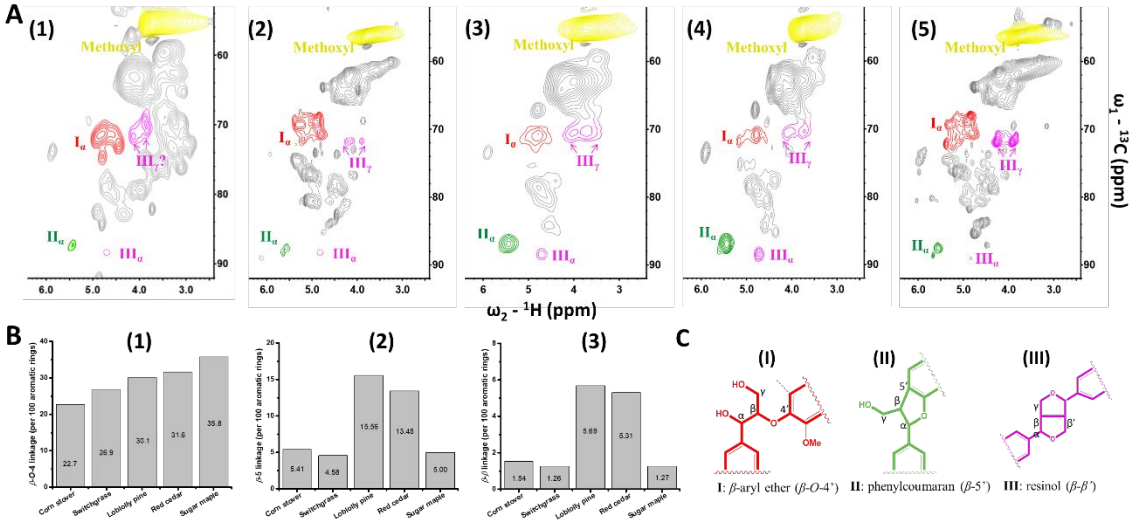

750

751 Fig. 7. Aliphatic regions of 2D ^{13}C–^{1}H (HSQC) NMR spectra. A, aliphatic regions of HSQC
752 spectra, where the assigned lignin linkages were highlighted in different colors. A1, A2, A3, A4,
753 and A5 were lignin from corn stover, switchgrass, loblolly pine, red cedar, and sugar maple,
754 respectively; B, the frequency of lignin linkages as measured by HSQC 2D NMR. B1, B2, and B3
755 were *β*-*O*-4, *β*-5, and *β*-*β* linkages, respectively, which were calculated based on 100 aromatic
756 rings; C, chemical structures of lignin linkages assigned in HSQC spectra.

757

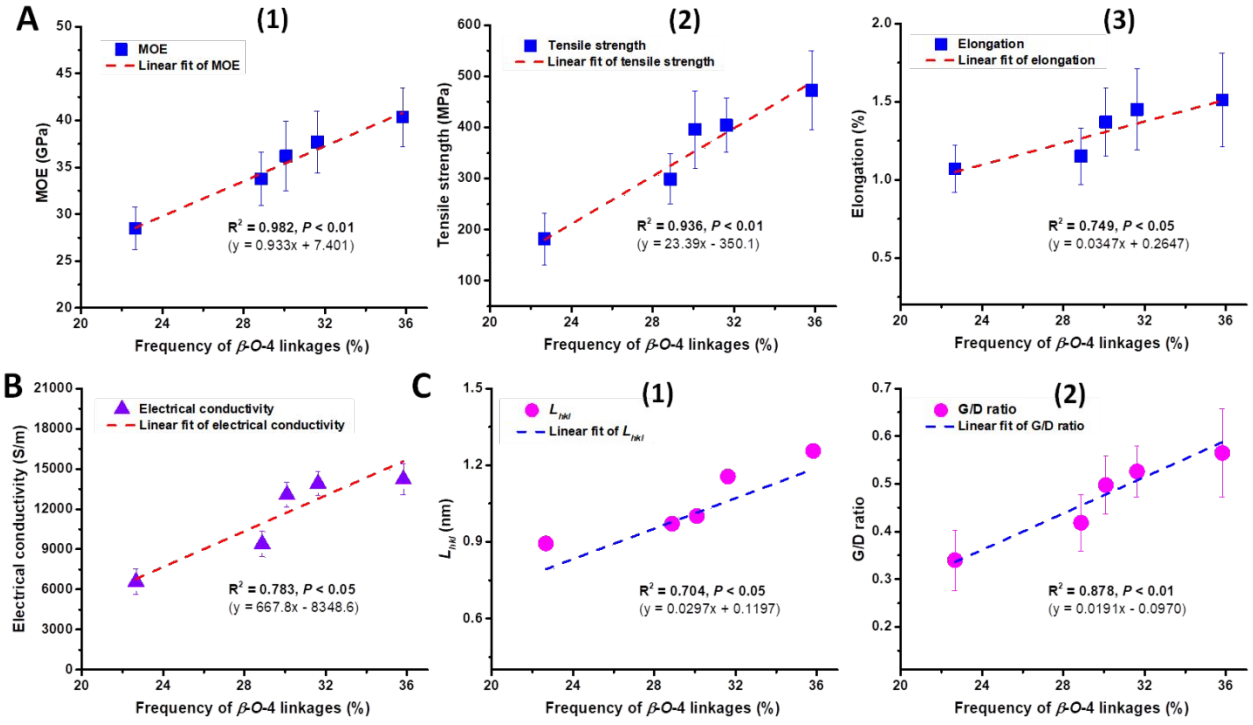

Fig. 8. The correlations of the lignin *β*-*O*-4 linkage with carbon fiber mechanical properties (A), electrical conductivity (B), and crystallite structures (C). A1, A2, A3 in Pane A are correlations of *β*-*O*-4 linkage with MOE, tensile strength, and elongation, respectively; C1 and C2 in Pane C were correlations of *β*-*O*-4 linkage with L_{hkl} and G/D ratio, respectively.